Rab8 Promotes Polarized Membrane Transport through Reorganization of Actin and Microtubules in Fibroblasts

Johan Peränen, Petri Auvinen, Hilkka Virta, Roger Wepf, and Kai Simons

European Molecular Biology Laboratory, Cell Biology Programme, D-69012 Heidelberg, Germany

Abstract. Rab8 is a small Ras-like GTPase that regulates polarized membrane transport to the basolateral membrane in epithelial cells and to the dendrites in neurons. It has recently been demonstrated that fibroblasts sort newly synthesized proteins into two different pathways for delivery to the cell surface that are equivalent to the apical and the basolateral post-Golgi routes in epithelial cells (Yoshimori, T., P. Keller, M.G. Roth, and K. Simons. 1996. *J. Cell Biol.* 133:247-256). To determine the role of Rab8 in fibroblasts, we used both transient expression systems and stable cell lines expressing mutant or wild-type (wt) Rab8. A dramatic change in cell morphology occurred in BHK cells expressing both the wt Rab8 and the activated form of the GTPase, the Rab8Q67L mutant. These cells formed processes as a result of a reorganization of both their actin filaments and microtubules. Newly synthesized vesicular stomatitis virus G glycoprotein, a basolateral marker protein in MDCK cells, was preferentially delivered into these cell outgrowths. Based on these findings, we propose that Rab8 provides a link between the machinery responsible for the formation of cell protrusions and polarized biosynthetic membrane traffic.

UNDERSTANDING how eukaryotic cells polarize their exteriors and interiors is one of the most important issues in cell biology. Extracellular signals and cell–cell contacts initiate the polarization through a cascade of events leading to reorganization of the plasma membrane and underlying cytoskeletal components (Nelson, 1992). Although cell types differ in function and cell architecture, most cells seem to be able to polarize during some stage of their life cycle. In epithelial cells, the plasma membrane is divided into apical and basolateral domains, containing different lipid and protein compositions. Correct transport and targeting of domain-specific proteins to the apical and basolateral membrane are crucial for the development and maintenance of epithelial polarity (Simons and Wandinger-Ness, 1990; Rodriguez-Boulan and Powell, 1992). Neurons also have two distinct surface domains, the axonal plasma membrane being equivalent to the apical domain of epithelial cells and the somatodendritic to the basolateral membrane (Dotti and Simons, 1990; Simons et al., 1993). In contrast with epithelial cells and neurons, nonmotile fibroblasts have no overt polarity. However, fibroblasts polarize when they become motile by acquiring a leading edge and a narrow tail (Singer and Kupfer, 1986). Most surprisingly, recent studies indicate that fibroblasts have two different biosynthetic routes from the TGN to the cell surface (Yoshimori et al., 1996), corresponding to the apical and basolateral pathways in MDCK cells. This finding raises the issue of how cytoskeletal elements regulate outgoing membrane traffic during cell polarization. It is known that microtubules play an important role in polarized membrane delivery in both epithelial cells and neurons. In epithelial cells, microtubules are required for apical and basolateral delivery (Rindler et al., 1987; Lafont et al., 1994). In neurons, intact microtubules are needed for axonal and dendritic delivery (Kelly, 1990; Cid-Arregui et al., 1995). In motile fibroblasts, newly synthesized membrane proteins are inserted at the leading edge in a microtubule-dependent fashion (Bergman et al., 1983; Rogalski et al., 1984). The role of actin in membrane trafficking is less well understood. However, there are indications that actin is involved in exocytosis and in apical endocytosis (Gottlieb et al., 1993; Muallem et al., 1995; Vitale et al., 1995). The growing list of myosin superfamily members, some of which are membrane bound, suggests that actin-based processes are involved in regulating membrane transport (see Hasson and Mooseker, 1995). In yeast there is evidence that a class V myosin, Myo2, has a role in polarized movement of vesicles into the forming bud (Govindan et al., 1995). Moreover, the existence of protein complexes, like dynactin, which can bind to microtubules and contains a short filament of an actin-related

J. Peränen and P. Auvinen contributed equally to this work.

Address all correspondence to Kai Simons, European Molecular Biology Laboratory, Cell Biology Programme, Meyerhofstrasse 1, D-69012 Heidelberg, Germany. Tel.: (49) 6221 387 334. Fax: (49) 6221 387 512.

J. Peränen and P. Auvinen's present address is Institute of Biotechnology, University of Helsinki, P.O. Box 45, FIN-00014; Helsinki, Finland.

protein, indicate that these two cytoskeletal elements could interact with each other (see Langford, 1995; Glotzer and Hyman, 1995).

In this paper, we have demonstrated a link between post-Golgi membrane traffic and cytoskeletal organization during the formation of cell protrusions in fibroblasts. The Rab8 GTPase seems to provide this connection.The Rab family of proteins, encompassing over 30 members, is involved in the regulation of membrane traffic between different membrane-bound compartments in the cell (Novick and Brennwald, 1993; Zerial and Stenmark, 1993). Rab8 is ubiquitously expressed (Chavrier et al., 1990) and is known to regulate biosynthetic traffic to the cell surface. The protein is localized in carrier vesicles derived from the TGN and on the plasma membrane (Huber et al., 1993*a*). In vitro assays have demonstrated that Rab8 acts on transport of newly synthesized vesicular stomatitis virus glycoprotein (VSV-G)[1] from the TGN to the basolateral plasma membrane in epithelial cells (Huber et al., 1993*a*). In hippocampal neurons, Rab8 regulates protein transport from the Golgi complex to the dendrites but not to the axons (Huber et al., 1993*b*). These results fit well with the findings that Rab8 can complement defective Ypt2p in *Schizosaccharomyces pombe* while Ypt2p rescues null mutants of Sec4p in *Saccharomyces cerevisae*; both of these yeast GTPases regulate membrane transport between the Golgi complex and the plasma membrane (Craighead et al., 1993; Haubruck et al., 1990). Here we have found that an activated mutant of Rab8 not only affects biosynthetic membrane traffic to the cell surface in BHK cells, but the mutant protein changes cell morphology as well. Cell protrusions are formed through a reorganization of both the actin and the microtubule networks and the vesicular transport routes.

Materials and Methods

DNA Constructs

We prepared Rab8 mutants, Rab8T22N and Rab8Q67L, using a PCR-based protocol (Ho et al., 1989). The mutant primers for Rab8Q67L were 5′-GGTCTAGAACGGTTTCGGACGATC-3′ and 5′-CCGAAACGGTTCTAGACCAGCTG, and for Rab8T22N 5′-CGGAGAAGCGGAACAGGACACAGTTCTTCCCCACCC-3′ (changed bases are underlined). T7 promoter primer and a Rab8-specific 3′-end primer 5′-GTCAAGCTTCACAGAAGAACACATCGG-3′ were used as outer primers in the amplifications. A point mutation, which changed Gln-60 to Arg, was observed in the original pGEM1-Rab8 plasmid (Huber et al., 1993*a*). Before using this plasmid as template, for creating the above-mentioned mutants, we corrected the point mutation to the wild-type (wt) form (wt-Rab8). All Rab8 PCR products were cleaved by BamHI and HindIII and cloned under the T7 promoter into pGEM1 cut with BamHI-HindIII, to create plasmids pRAB8-wt, pRAB8-T22N, and pRAB8-Q67L. All PCR-amplified genes were sequenced to verify the mutations and to exclude PCR errors.

The wild-type gene of VSV-G in plasmid pSVGL (Rose and Bergman, 1983) was cut out by BamHI and inserted under the T7 promoter by cloning it into the BamHI site of pGEM-1, creating plasmid pGEM-G. To obtain plasmid pGEM-HA, we cloned a BamHI fragment, encoding the hemagglutinin (HA) gene (WCN/33/HI) of the influenza A WSN strain from plasmid pBR-HAX (a generous gift from D. Nayak, University of California/Los Angeles; Hiti et al., 1981) into the BamHI site of pGEM-1. Plasmid pBK-RAB867L was obtained by cloning the Rab8Q67L gene (processed by BamHI [blunt]-HindIII) from pRAB8-Q67L into the cytomegalovirus promoter–based vector pBK-CMV (Stratagene, La Jolla, CA), which had been cut with NheI(blunt) and HindIII. Plasmid pMXR-67L was created by cloning the Rab8Q67L gene, as a BamHI-HindIII cut and blunted fragment, into the SnaBI site of the MX promoter–based vector pMX-Neo-1. Plasmids pSFV-RAB8-wt, pSFV-RAB8-22, and pSFV-RAB8-67 were constructed by cloning the corresponding Rab8 genes (BamHI-HindIII, blunted) into the SmaI site of the Semliki Forest virus (SFV)–based replicon vector pSFV1 (Liljeström and Garoff, 1991). To obtain recombinant Rab8 protein for immunization, we cloned the wt-Rab8 gene into the BamHI and HindIII sites of the *Escherichia coli* expression vectors pDAT-1 and pGAT-1, creating pDAT-Rab8 and pGAT-Rab8. We likewise cloned the Rab8T22N and Rab8Q67L genes into the pGAT-1 vector, creating pGAT-Rab8T22N and pGAT-Rab8Q67L. These vectors contain a modified T7*lac* promoter and a fusion partner consisting of either a his6-dihydrofolate reductase (DHFR) (his6-DHFR) gene (pDAT-1) or a his6-glutathionine-*S*-transferase (GST) (his6-GST) gene (pGAT-1).

GTP Overlay

Rab8 or its mutants were expressed in *E. coli* JM109(DE3) cells harboring corresponding constructs pGAT-Rab8, pGAT-Rab8T22N, and p-GAT-Rab8Q67L. Proteins from the lysates of these cells were separated by SDS-PAGE and transferred to nitrocellulose (Huber et al., 1993*b*). The blots were incubated with [alfa P32-GTP] according to Huber et al. (1993*b*). GTP binding was visualized by autoradiography using Kodak Xomat Ar film with an intensifying screen (Eastman Kodak Co., Rochester, NY).

Preparation of Antisera

JM109(DE3) cells (Promega, Madison, WI) harboring either pDAT-Rab8 or pGAT-Rab8 were cultured at 37°C in 0.5 liter of Luria broth medium with ampicillin (200 μg/ml). Expression was induced by addition of isopropylthio-β-D-galactoside to 0.5 mM at a OD_{600} of 0.7. The cells were harvested after a 3-h induction period, and the purification was done under denaturing conditions by using a Ni^{2+}-nitrilotriacetic acid column (2 ml) according to the manufacturer (Qiagen, Hilden, Germany). One-tenth of the eluted his6-GST-Rab8 protein was precipitated by diluting it tenfold in PBS (Ca^{2+} and Mg^{2+} free) and by centrifuging it at 13,000 rpm for 5 min. The obtained pellet was rinsed once with PBS, and then resuspended in PBS containing 1% SDS. After solubilization, the protein was diluted tenfold with PBS, lowering the SDS concentration to 0.1%. The purified protein in PBS–0.1% SDS was used directly to raise antibodies in rabbits. For affinity purification of antisera, his6-DHFR-Rab8 was separated by SDS-PAGE and transferred onto nitrocellulose filters (Peränen, 1992). The protein was visualized by Ponceau staining, and the band was cut out as a strip. The strip was then blocked by incubating it for 1 h at 4°C in PBS containing 15% FCS. The antisera (300 μl) was applied to the strip in 5 ml of PBS containing 10% FCS and incubated overnight at 4°C. After washing five times with PBS and once with H_2O, the antibodies were eluted as previously described (Peränen, 1992). His6-DHFR-Rab8 was used instead of his6-GST-Rab8 to get rid of antibodies directed against GST.

Cell Culture and Transient Transfections

BHK cells (strain CCL10; American Type Culture Collection, Rockville, MD) were grown in Glasgow's modified medium, supplemented with 5% FCS, 2 mM glutamine, 100 U/ml penicillin, 10 g/ml streptomycin, and 10% tryptose phosphate broth at 37°C in 5% CO_2. For immunofluorescence microscopy, cells were split 18–24 h before transfection, and for labeling studies, 36–48 h.

Transient expression using the T7 RNA polymerase–recombinant vaccinia virus (vTF7.3) was done as previously described (Fuerst et al., 1986; Bucci et al., 1992). Shortly, the cells were washed twice with PBS+ (PBS containing 1 mM $CaCl_2$ and 1 mM $MgCl_2$) and infected with 5–10 plaque-forming units (pfu) per cell at 37°C for 30 min with intermittent agitation. The cells were then washed twice with PBS+ and transfected using Lipofectin™ reagent according to the manufacturer's instructions (GIBCO BRL, Gaitherburg, MD) in the presence of 10 mM hydroxyurea (Bucci et al., 1992). For immunofluorescence microscopy and labeling studies, we used 9 μl Lipofectin™ and 2 μg plasmid per 35-mm plate. The plasmids pRAB8-wt and pRAB8-Q67L are cytotoxic after prolonged incubation. To minimize the cytotoxicity, we restricted our experiments below 4 h af-

1. *Abbreviations used in this paper*: DHFR, dihydrofolate reductase; ECL, enhanced chemiluminescence; GST, glutathione-*S*-transferase; HA, hemagglutinin; MTOC, microtubule organizing center; SFV, Semliki Forest virus; TX-114, Triton X-114; VSV-G, vesicular stomatitis virus glycoprotein; wt, wild type.

ter transfection. Morever, in double transfections, for immunofluorescence studies, we used the pRAB8 plasmids and pGEM-G plasmid in a 1:4 ratio, and in labeling studies, in a 1:2 ratio. Although less pRAB8 plasmids were used, ~90% of the positive cells expressed both proteins as observed by immunofluorescence microscopy. In additional double transfections with pGEM-G and pGEM-HA, we used the plasmids in a 1:2 ratio.

Transient expression of Rab8 proteins was also done using the Semliki Forest virus–based expression system (Liljeström and Garoff, 1991). The pSFV-Rab8-wt, -T22N, and -Q67L plasmids were linearized with SpeI, and RNA was produced from the plasmids via SP6 RNA polymerase–driven run-off transcription (Liljeström and Garoff, 1991). The RNA was purified free from nucleotides using the RNeasy total RNA kit (Qiagen). 2 μg of purified RNA was mixed with 10 μl of Lipofectin™ in 1 ml of Optimem (GIBCO BRL) and applied onto cells on a 35-mm plate. During the first hour of incubation, the cells were agitated every 10 min.

Stable Transfectants

BHK cells on 100-mm plates were transfected with 15 μg of either pBK-CMV (control), pBKCMV-Rab8 67L, or pMXR-Rab8 67L plasmids using 50 μl Lipofectin™ in Optimem according to the manufacturer (GIBCO BRL). After a 5-h incubation, Optimem was changed to Glasgow's modified Eagle's medium supplemented with 10% FCS (see above), and the incubation was continued for 20 h. The next day the cells were trypsinized and plated at different dilutions on 100-mm plates in Glasgow's modified Eagle's medium containing 500 μg of G418 per ml. Clones were isolated 14 d later and characterized by Western blotting and immunofluorescence microscopy. Clones were selected on the basis of expression, and two were used for detailed characterization: CMV Rab8 67L was called cell line **a**, and MX Rab8 67L was called cell line **b**.

Western Blots and Phase Separation

When the Rab8 amount was compared between different stable cell lines and control cells, cells were scraped from the plates and washed in PBS, and the protein concentration was determined by protein assay (Bio Rad Laboratories GmbH, München, Germany). Equal amounts of total proteins from different cell lines were then separated by 12% SDS-PAGE. Triton X-114 (TX-114) phase separation was done according to Bordier (1981). Shortly, control cells or pSFV-wt-Rab8, -T22N, and -Q67L transfected cells on 35-mm plates were lysed in buffer D (1% TX-114, 20 mM Tris-HCL, 150 mM NaCl, 25 μg/ml each of chymostatin, leupeptin, antipain, and pepstatin A [CLAP], pH 7.5) by a 10-min incubation on ice. Nuclei and aggregates were pelleted at 13,000 rpm for 5 min at 4°C. Phase separation was done by incubating the supernatant 3 min at 37°C and centrifuging 1 min at 8,000 rpm; the detergent phase was resuspended in the inital volume using buffer D without TX-114, and TX-114 was added to the aqueous phase to a final concentration of 1%. The phase separation was repeated for both samples. After adjusting the volume of the samples, equal amounts were separated on 12% SDS-PAGE.

The proteins were then transferred to nitrocellulose as described previously (Ikonen et al., 1995). Rab8 was detected by using affinity-purified anti-Rab8 antibodies diluted 1:500, and VIP21/caveolin was detected using anti-caveolin polyclonal antibody (Santa Cruz Biotechnology, Inc., Santa Cruz, CA) diluted 1:2,000, in combination with HRP-conjugated anti–rabbit IgG and enhanced chemiluminescence (ECL) (Amersham Intl., Little Chalfont, UK).

Cell Surface Transport

For transport studies we used T7 vaccinia–based double transfections combining pGEM-G with either pRAB8-T22N or pRAB8-Q67L. 3 h after transfection, the cells were pulsed with 80 μCi ^{35}[S]methionine per 35-mm plate in MEM lacking methionine for 10 min. After the pulse, some cells were immediately put on ice, while the others were chased in the presence of 20-fold excess of cold methionine for indicated time periods. The cells were then washed twice with PBS$^+$ and surface biotinylated by incubating for 30 min in 0.5 ml PBS$^+$ with 1 mg/ml N-hydroxysuccinimido–LC-biotin (Pierce, Oud-Beijerland, The Netherlands). After biotinylation, the cells were washed once with PBS$^+$, and then incubated, twice for 5 min each, in PBS$^+$ containing 0.1 M glycine and 0.3% BSA. They were washed twice with PBS before lysis in 1 ml NET buffer (2% NP-40, 20 mM Tris-HCl, 150 mM NaCl, CLAP; pH 7.5) by a 10-min incubation on ice. The lysate was removed by a micropipette from the plate, without scraping the cells. The lysate was centrifuged at 13,000 rpm for 5 min at 4°C to get rid of aggregates. 500 μl of the supernatant was incubated with 5 μl rabbit anti–VSV-G antibodies overnight at 4°C. Antigen–antibody complexes were bound to 200 μl of a 20% slurry of protein A–Sepharose 4B (Pharmacia, Uppsala, Sweden) in NET buffer for 60 min at room temperature. The beads were washed five times during 60 min with NET buffer. Antigen was released by boiling the beads in 50 μl 1× Laemmli sample buffer for 2 min. The antigen was then diluted in 700 μl buffer B (2% NP-40, 0.2% SDS, 20 mM Tris-HCl, CLAP, pH 7.5), 30 μl of streptavidin agarose (Pierce) was added, and the mix was incubated overnight by rotation at 4°C. The supernatant was moved to another tube representing unbound internal VSV-G proteins, while the VSV-G bound to the streptavidin agarose represented surface VSV-G. The beads were washed, and the bound protein was eluted as described previously (Brändli et al., 1990). The supernatant was concentrated by using a phenol-ether method described by Sauve et al. (1995). The samples were separated by 10% SDS-PAGE and processed for fluorography. The bands corresponding to VSV-G were scanned with the PhosphorImager (Applied Biosystems, Foster City, CA), the band intensities were quantitated with ImageQuant software (Molecular Dynamics, Sunnyvale, CA), and transport was standardized for amounts of total VSV-G.

Immunofluorescence and Video Microscopy

All cells grown on coverslips were fixed with 4% paraformaldehyde in PBS$^+$ for 15 min, and free aldehyde groups were quenched with 50 mM NH_4Cl in PBS for 10 min. After fixation, the cells were permeabilized with 0.1% Triton X-100 in PBS for 10 min. The cells were first incubated for 30 min at room temperature with primary antibodies diluted in 0.2% gelatin-PBS, whereafter the cells were rinsed four times with gelatin-PBS for 30 min. The secondary antibodies were applied to the cells in the same way. After the last wash, the cells were refixed with 4% paraformaldehyde, followed by quenching with 50 mM NH_4Cl for 5 min. The cells were observed with a fluorescence microscope (Axiophot, Zeiss, Oberkochen, Germany). The affinity-purified anti-Rab8 was diluted 1:20, the anti-α-tubulin 1:100 (Amersham Intl.), and polyclonal anti–VSV-G 1:400; monoclonal anti-HA and rhodamine-phalloidin (Molecular Probes, Inc., Eugene, OR) were diluted to 1 U/ml. As secondary antibodies we used FITC- or TRITC-conjugated goat anti–rabbit antibodies and FITC- or TRITC-conjugated rat anti–mouse antibodies (Dianova GmbH, Hamburg, Germany).

Stably transfected cells grown on coverslips were infected with 30 pfu/ml of VSV ts045 virus or with 30 μm/ml of influenza WSN ts61 for 1 h at 32°C, followed by a 2.5 h incubation at 39.5°C as described before (Wandinger-Ness et al., 1990). Then coverslips were transferred to 32°C, and cells were fixed (see above) at different time points (0, 15, 30, 45, and 90 min). After quenching and blocking with 0.2% gelatin, a polyclonal rabbit antiserum against VSV- G (1:400) was added and incubated as mentioned above. Samples were incubated with secondary antibody, washed, and refixed. Afterward, quenching samples were treated with 0.1% Triton X-100 for 1 min, washed with PBS, and blocked with gelatin, followed by incubation with mAb 17.2.21.4 against VSV-G (1:50). After the washes, secondary antibody was added and incubated as above for 30 min. Then samples were washed and mounted for observation. For analyzing the delivery of the WSN ts61 HA, the cells were fixed and permeabilized as above, and then stained with an mAb against HA (Wandinger-Ness et al., 1990). Video microscopy was performed as previously described (Huber et al., 1995).

Low Voltage Scanning EM

For scanning EM imaging, cells were plated onto 11-mm coverslips or 3-mm sapphire discs (diam = 0.05 mm; Bruegger SA, Switzerland), which were previously coated with 20 nm of carbon. The cells were cultivated as described for light microscopy. Such samples were chemically fixed for 5 min at room temperature with 4% formaldehyde solved in PBS. Samples were then dehydrated through an ethanol series and washed three times in 100% water-free ethanol before freezing. For freezing, the samples were then plunge frozen into liquid nitrogen and freeze dried at −90°C for 2 h in a self-constructed high vacuum cryopreparation chamber (Wepf, R., manuscript in preparation). After freeze drying, the samples were rendered conductive by planar magnetron sputter coating with tungsten to an average film thickness of 2 nm, and subsequently high vacuum cryotransferred into a FESEM (XL-30 FEG; Philips Electronic Instruments, Inc., Mahwah, NJ) equipped with a cryo-stage preset at a temperature of −100°C. Scanning electron images were taken at 5 kV and at a specimen temperature of −100°C. Scanning EM images were recorded digitally and printed on a Kodak ES printer (Eastman Kodak Co.).

Results

To determine whether mutations in Rab8 affect Golgi to cell surface transport in BHK cells, two different mutants were generated. One of the mutants, Rab8T22N, contains a threonine to asparagine substitution at residue 22, in the first GTP/guanosine diphosphate (GDP)-binding motif. In ras and other rab proteins, this mutant has a lower affinity for GTP than for GDP (Feig and Cooper, 1988; Stenmark et al., 1994). It also appears to sequester guanine nucleotide exchange factors (Burstein et al., 1992), and thereby has a dominant negative effect on the function of the endogenous GTPase. The other mutant, Rab8Q67L, contains a glutamine to leucine substitution at residue 67. The corresponding mutation in p21-ras and other small GTPases inhibits both the intrinsic and GAP-stimulated GTPase activity (Der et al., 1986; Stenmark et al., 1994) and produces an activated form of the GTPase. By a GTP overlay assay, we confirmed that normal Rab8 (wt-Rab8) and Rab8Q67L bind GTP, whereas Rab8T22N did not as expected (data not shown). We expressed normal Rab 8 (wt-Rab8) and mutant cDNAs by using the vaccinia T7 system (vT7) (Fuerst et al., 1986; Bucci et al., 1992) in BHK cells (Fig. 1 *A*) and also in stably transfected cell lines (see Materials and Methods) (Fig. 1 *B*). The isoprenylation of the expressed Rab8 proteins was monitored by extracting the proteins from cells by the detergent Triton X-114 followed by phase separation. After expression, wt-Rab8, Rab8T22N, and Rab8Q67L were predominantly found in the detergent phase, indicating that they were isoprenylated (Fig. 2).

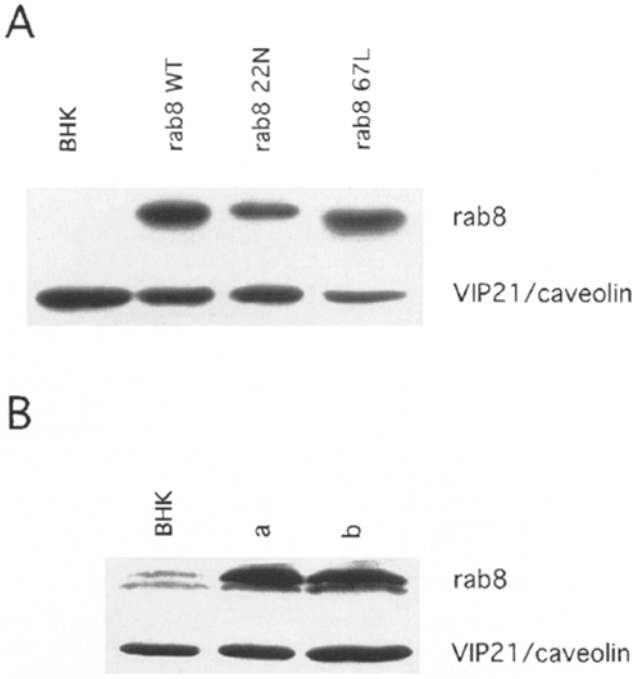

Figure 1. Expression of Rab8 and Rab8 mutants in BHK cells. (*A*) Cell lysates were prepared from BHK cells that were infected with the vT7 virus and transfected with wt-Rab8 (lane *2*), Rab8T22N (lane *3*), or Rab8Q67L constructs (lane *4*). Nontransfected BHK cells were used as controls (lane *1*). (*B*) Cell lysates were prepared from BHK cells (lane *1*) and the BHK clone **a** cells (lane *2*) and BHK clone **b** cells (lane *3*) (see Material and Methods). Cells were lysed, and equal volumes of the lysates were run on SDS-PAGE and transferred to nitrocellulose filters. The filter was first blotted with anti-Rab8 antibody and then with anti-VIP21/caveolin antibody. Detection with combination at HRP-conjugated anti-rabbit IgG and ECL.

Transport of VSV-G to the Cell Surface in Cells Expressing the Rab8 Mutants

To study the effect of Rab8 on membrane trafficking to the cell surface, we used VSV-G as a tool because we previously showed that the transport of this protein to the polarized cell surface is regulated by Rab8 in epithelial cells and neurons (Huber et al., 1993*a*, *b*). VSV-G is basolateral in MDCK cells and somatodendritic in hippocampal neurons. By placing the Rab8 genes and the VSV-G gene under the T7 promoter, we were able to use the T7 RNA polymerase recombinant vaccinia virus expression system (Fuerst et al., 1986). The advantage with this system is that two genes can be coexpressed, making it possible to study processes involving more than one expressed protein. After 3 h of transfection, cells were pulsed with ^{35}[S]methionine for 10 min, and then chased for either 0 min or 60 min (Fig. 3). The appearance of VSV-G on the cell surface was monitored by using a method based on cell surface biotinylation and immunoprecipitation (see Materials and Methods). Cells transfected only with the VSV-G plasmid served as controls. We compared the amounts of VSV-G that were transported to the cell surface during the 60-min chase period. Expression of rab8T22N decreased the transport by 20.1% (two experiments: 18.7%; 21.5%) during the 60-min chase, while Rab8Q67L decreased it by 29.5% (two experiments: 28.8%; 30.2%) as compared with the cells that were not transfected with Rab8 constructs. This indicates that the Rab8 mutants do influence the transport of VSV-G, but the effects are not dramatic (see below).

Effects of Rab8 on Cell Shape

We observed that transient expression of Rab8 led to a drastic change of cell morphology (Fig. 4). To further elu-

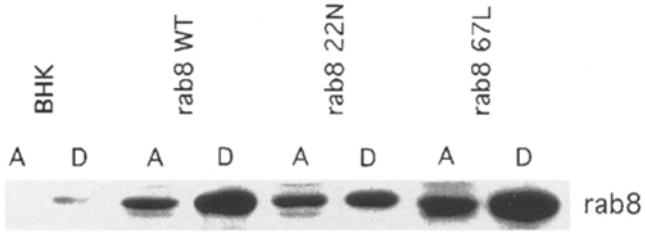

Figure 2. Isoprenylation of Rab8 in BHK cells. BHK cells grown in dishes were infected with vT7 virus and transfected with wt-Rab8 , Rab8T22N, or Rab8Q67L constructs. Nontransfected BHK cells served as controls. After 3 h of expression, cells were treated with buffer D (see Materials and Methods). After Triton X-114 phase separation, equal amounts of samples from the aqueous phase (*A*) and the detergent phase (*D*) were run on PAGE and transferred to nitrocellulose filters followed by blotting with Rab8 antibody. Detection with combination at HRP-conjugated anti-rabbit IgG and ECL.

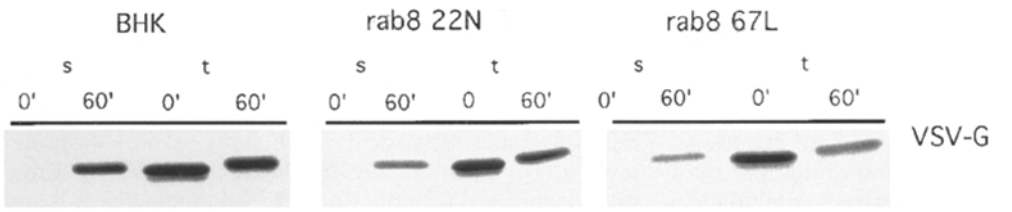

Figure 3. Transport of VSV-G to the cell surface in cells expressing the Rab8 mutants. BHK cells grown in dishes were infected with vT7 virus and transfected with pGEM-G and with Rab8T22N or with Rab8Q67L constructs. BHK cells transfected with only pGEM-G (marked BHK) served as controls. After 3 h of transfection, cells were pulsed with [^{35}S]methionine followed by a chase of 0 (*0'*) and 60 min (*60'*). At the end of the chase, the cell surface was biotinylated. After biotinylation, cells were lysed and VSV-G was collected by immunoprecipitation (see Materials and Methods). Biotinylated (*s*, surface) and cellular (*t*, total) VSV-G were separated and run on PAGE, and band intensities were quantified with the PhosphorImager.

cidate this observation, we expressed our Rab8 mutants and the wt-Rab8 in BHK cells, using either the vT7 system or the SFV expression system. The latter system was used as an alternative expression vector to exclude possible effects resulting from the vT7 system itself. Typical BHK cells are mostly flat and triangular (Fig. 4 *A*). Expression of Rab8T22N with these vectors had no profound effect on cell shape (data not shown), even after longer transfection periods (up to 5 h). However, when Rab8Q67L, the activated mutant, was expressed, a dramatic change in the cell morphology was observed. This change was usually associated with the formation of cell protrusions (Fig. 4). These processes sometimes extended >100 μm from the cell body. Observation of many cells, also by video microscopy (not shown), demonstrated that these processes were clearly produced by active outgrowth and not derived from cells moving forward and leaving extensions behind. When the vT7 system was used, morphological changes were apparent already at 2 h after transfection (as soon as rab8 began to be expressed), and with the SFV vector,

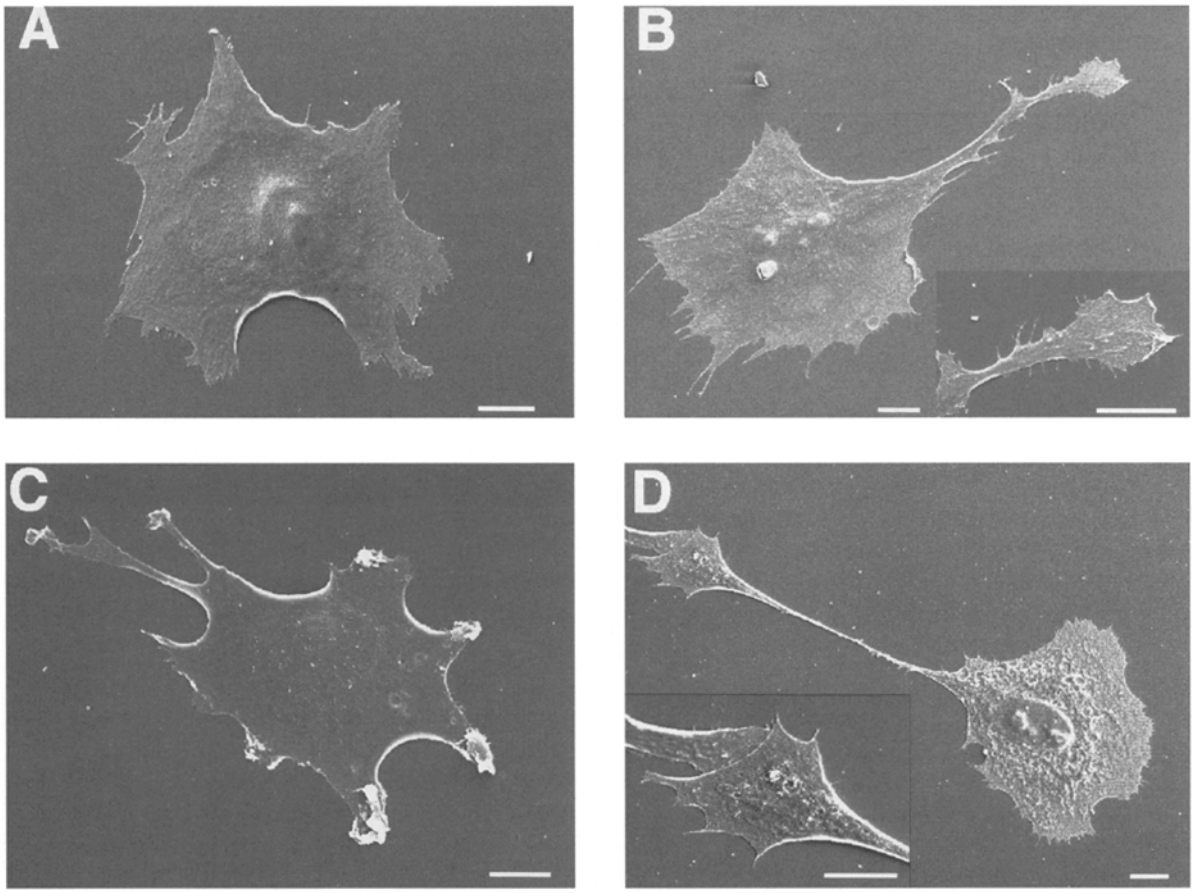

Figure 4. Morphology of the RabQ67L-expressing cells differs from the parental BHK cells. BHK cells and BHK clone **a** cells (see Materials and Methods) were grown on coverslips, and samples were prepared for low voltage scanning EM. BHK cells were infected with vT7 virus and transfected with the Rab8Q67L construct for 3 h. (*A*) A BHK cell showing a representative normal cell shape. (*B*) BHK clone **a** showing a long process. (*C*) BHK clone **a** with membrane lamellae and ruffles. (*D*) BHK cell expressing Rab8Q67L by the vT7 system displaying a long cell process. Bar, 10 μm.

changes were seen at ~3–4 h after transfection. Also, expression of wt-Rab8 leads to similar changes in cell shape although the effects were not as dramatic as those for Rab8Q67L (data not shown). Expression of Rab5 and Rab10 by the vT7 system in BHK cells had no effect on cell shape even 5 h after transfection, indicating that the morphological changes seen with Rab8 are not common to other Rab proteins.

To avoid problems that could be associated with virus vector systems, we generated stable BHK cell lines expressing the Rab8Q67L mutant. We inserted the Rab8Q67L gene either under the CMV or MX promoter. After transfection, clones resistant to neomycin were selected. Two clones were further characterized, CMV67L-5 and MX-67L-9, which were called **a** and **b** (see Materials and Methods). Immunoblot analysis of these cell lines demonstrated that clone **a** expressed Rab8 10-fold, and clone **b** fivefold over the endogenous Rab8 level (Fig. 1 B). Morphological analysis showed that ~20% of the control cells contained cell protrusions, while ~50% of the clone **b** cells (data not shown) and as many as 90% of the clone **a** cells had processes (Table I). Moreover, the number of processes per cell, as well as the length of the processes, was increased in cells expressing the activated Rab8 (Table I). Taken together, these data demonstrate that expression of Rab8Q67L promotes the formation of cell protrusions in BHK cells. Similar results were obtained using either virus vectors for expression or stably transfected cells.

Polarized Transport of VSV-G in Rab8Q67L-expressing BHK Cells

The appearance of cell protrusions in Rab8-expressing cells raised the question whether biosynthetic membrane transport was directed into these processes. To answer this question, we coexpressed the VSV-G gene with the Rab8 mutant genes, using the vT7 system, and studied their distributions in the cell by immunofluorescence microscopy. Cycloheximide was added to the transfected cells for 30 min 3 h after transfection to chase out newly synthesized VSV-G from the ER into the Golgi complex and to the plasma membrane.

When control cells were transfected with the VSV-G plasmid, the VSV-G proteins were found mostly in the perinuclear region and on small vesicular structures, and evenly distributed on the plasma membrane as expected from numerous previous studies (Bergman et al., 1983; Kreis, 1986). The localization of endogenous Rab8 was difficult to visualize because of the low level of Rab8 present in these cells. However, Rab8 could be weakly seen on numerous vesicular structures as previously described (Huber et al., 1993*b*). When the VSV-G plasmid was coexpressed with the Rab8T22N mutant (Fig. 5, *A* and *B*), the VSV-G distribution was similar to that seen in cells only expressing VSV-G (data not shown), the staining being mainly perinuclear (Fig. 5 *B*) and on the plasma membrane when cell surface VSV-G was visualized on fixed cells (data not shown). However, to our surprise Rab8T22N was localized to the nuclear envelope and to structures reminiscent of ER in these cells (Fig. 5 *A*). The Rab8T22N molecule was hardly seen in the Golgi region or at the plasma membrane.

The reason for the mislocalization is not known, but we assume that the mislocalized Rab8T22N was not capable of sequestering proteins interacting with Rab8, thus explaining why this potentially dominant negative mutant was almost inactive in inhibiting VSV-G transport (Fig. 3). We therefore used the Rab8T22N mutant as a convenient control in the analysis of the effects of the activated Rab8 mutant on cell morphology and membrane transport.

We next determined the effect of Rab8Q67L on VSV-G distribution, using the same conditions as for Rab8T22N. As mentioned above, cells expressing either wt-Rab8 or activated Rab8 had an altered shape characterized by outgrowth of processes. In these cells, VSV-G was localized to the perinuclear region and to numerous small dots found in the processes, with increasing staining toward the tips of the protrusions (Fig. 5, *D* and *H*). Rab8 was enriched in the same cell surface outgrowths in which VSV-G labeling was seen (Fig. 5, *arrowheads*), but it was weak or absent in other peripheral regions of the cell early after transfection (Fig. 5, *C*, *E*, and *G*). Some Rab8 staining could also be seen in the perinuclear region (Fig. 5, *C* and *E*). In contrast with Rab8T22N, wt-Rab8 and Rab8Q67L showed little nuclear envelope and ER-like staining. On the cell surface, VSV-G was seen all over the plasma membrane 4–4.5 h after transfection (data not shown).

To analyze the surface appearance of VSV-G in more detail, we used the temperature-sensitive mutant of VSV-G, ts045, to follow the delivery of newly synthesized VSV-G to the cell surface. With this virus mutant, it is possible to accumulate VSV-G in the ER at the nonpermissive

Table I. Determination of Process Formation and Viral Glycoprotein Accumulation

	Process-positive cells*	Cells with prominent processes‡	Accumulation of VSV-G in processes§	Accumulation of HA in processes‖
	%	%	%	%
BHK	17.8 ± 2.3 (132)¶	5.7 ± 0.4 (189)		
BHK clone **a**	91.1 ± 1.6 (126)	46.0 ± 1.5 (122)	93.6 ± 1.4 (46)	15.1 ± 3.8 (575)

The percentage of cells with processes was calculated from two separate experiments. Data are the mean ± SEM values.

*Process-positive cells are defined as cells having processes at least half the length of the cell body.

‡Cells with processes longer than the body cell were considered as having prominent processes.

§BHK clone **a** cells were infected with vT7 and transfected with the VSV-G construct as described in the legend to Fig. 5, and used for the determination of VSV-G accumulation. The percentage of process-positive cells showing VSV-G accumulation in the process was calculated from two separate experiments.

‖BHK clone a cells were infected with influenza WSN ts61 at 32°C for 1 h, infection was continued at 39.5°C for 2 h and 15 min. Then cycloheximide (20 μg/ml) was added, and incubation continued for 30–40 min at 32°C. The cells were fixed, permeabilized, and stained with anti-HA antibodies. Accumulation of HA in the cell processes was determined and calculated from three experiments as was done for VSV-G.

¶Total number of cells are in parentheses.

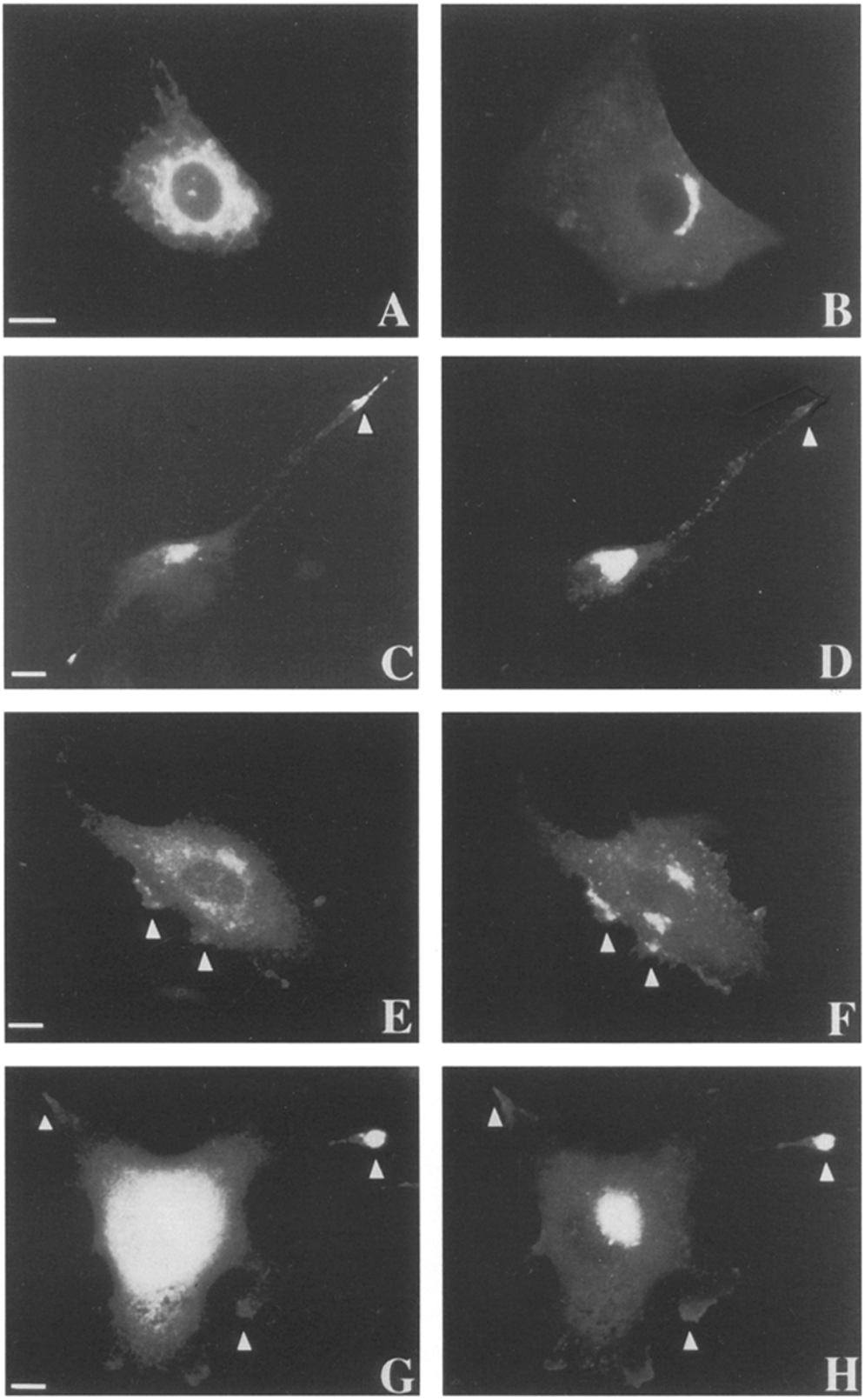

Figure 5. Distribution of VSV-G and Rab8 in cells overexpressing wt-Rab8, Rab8T22N, and Rab8Q67L. BHK cells were infected with vT7 virus and cotransfected with the VSV-G and Rab8T22N (*A* and *B*), Rab8Q67L (*C* and *D*), or wt-Rab8 (*E–H*) plasmids. Cycloheximide was added to the cells 3 h after transfection. At 3.5 h after transfection, the cells were fixed, permeabilized, and doubly stained with anti-Rab8 antibodies (*A*, *C*, *E*, and *G*) and anti-VSV-G antibodies (*B*, *D*, *F*, and *H*). (*Arrows*) Examples of regions where Rab8 and VSV-G colocalize. The cell in *G* and *H*, wt-Rab8, is so overexpressed that also cytosolic staining is seen. Bar, 10 μm.

temperature, 39°C. Synchronized delivery of the VSV-G to the cell surface can then be initiated by lowering the temperature to 32°C. We followed delivery by first labeling the surface VSV-G with the rabbit antibody, and then we permeabilized the fixed cells by Triton X-100 to label the intracellular VSV-G by an mAb. In BHK cells, newly synthesized VSV-G was seen all over the surface after allowing transport from the ER to proceed for 45 min (Fig. 6 *B*). In contrast, delivery of newly synthesized ts045 VSV-G was preferentially to the cell processes in the BHK clone **a**

cells that express activated Rab8. In the cell observed in Fig. 6 *D*, we have caught delivery of VSV-G to the cell process before lateral diffusion of VSV-G has spread it over the plasma membrane. After 90 min of transport, VSV-G is seen on the whole surface (Fig. 6 *F*). Quantitation of cells demonstrated that >90% of the cells preferentially deliver VSV-G into cell processes (Table I). These data demonstrated a dramatic polarity of VSV-G delivery in cells expressing activated Rab8.

To find out whether an apical cognate marker, the influenza virus hemagglutinin, is also preferentially directed from the Golgi complex to the cell protrusions, we performed the same experiments as those for expressing the VSV-G protein. Analysis of HA distribution after double transfection of BHK clone **a** cells with VSV-G and HA-encoding constructs showed no overt polarity in delivery. The HA seemed to be delivered more uniformly to the cell surface in comparison with VSV-G delivery. The typical accumulation as seen for VSV-G (Fig. 7 *A*) at the tip of the long process was not observed (Fig. 7 *B*). Quantitation after transport of a temperature-sensitive HA molecule from the ER to the cell surface after infecting BHK clone **a** cells with influenza WSN ts61 demonstrated that 85% of the infected cells showed no preferential accumulation of HA in the cell processes (Fig. 8; Table I). These data show that basolateral and apical cognate marker glycoproteins are handled differently in Rab8Q67L-expressing BHK cells.

Redistribution of Actin and Microtubules in Rab8Q67L-expressing Cells

Changes in cell morphology are usually caused by reorganization of the cellular cytoskeleton. We therefore wished to determine whether Rab8 expression caused rearrangement of the actin cytoskeleton. We identified transfected cells by elevated Rab8 immunoreactivity (Fig. 9, *A* and *C*). Expression of Rab8T22N in BHK cells did not change the organization of actin filaments from that seen in control cells. In these cells, the actin cytoskeleton contained abundant stress fibers (Fig. 9 *B*). In contrast, expression of Rab8Q67L caused a dramatic redistribution of the actin cytoskeleton. The stress fibers disappeared and actin was relocalized to the newly formed cell processes and lamellae (Fig. 9 *E*) where it colocalized with overexpressed Rab8 (Fig. 9, *C* and *D*). Similar changes were seen in cells

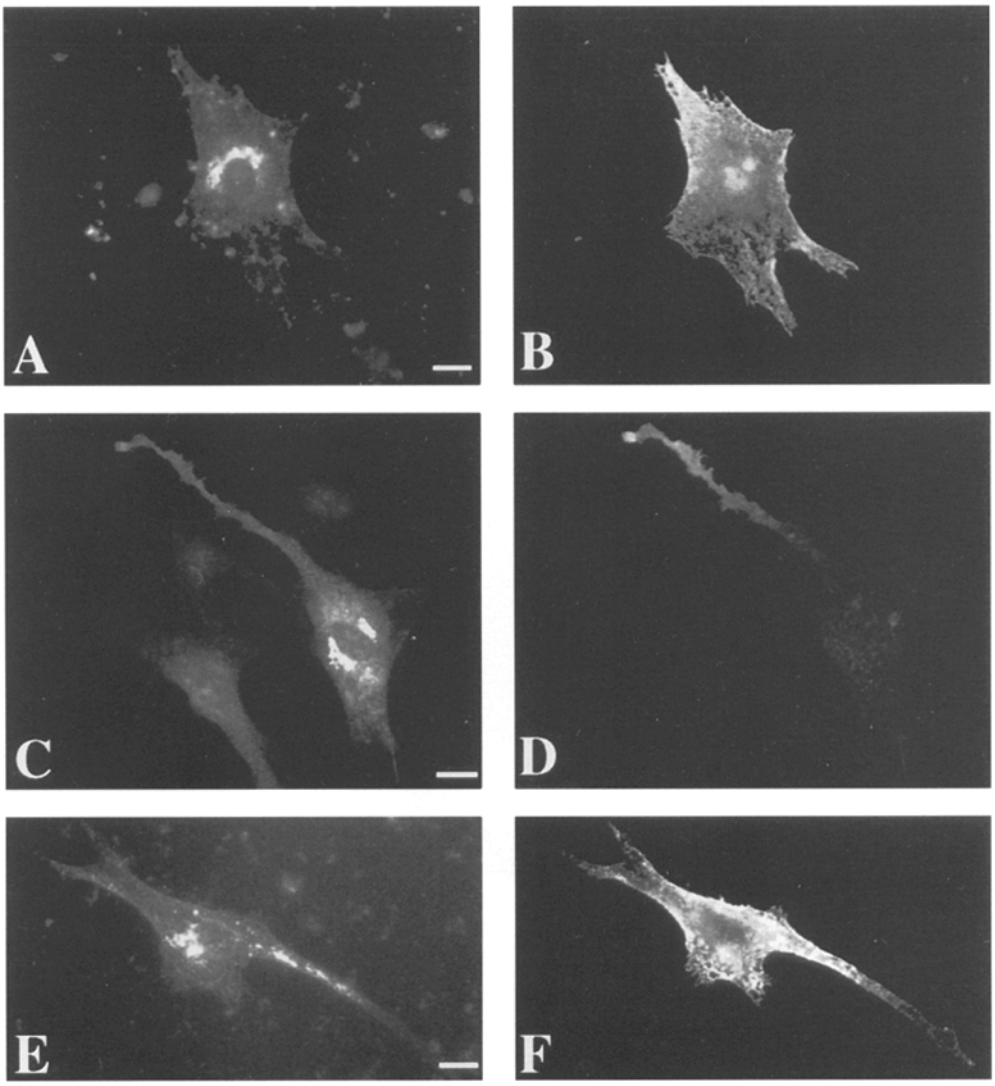

Figure 6. Delivery of newly synthesized VSV-G protein to the cell surface in BHK and BHK clone **a** cells. BHK (*A* and *B*) and BHK clone **a** cells (*C–F*) were grown on coverslips and infected with VSV ts045 virus for 1 h at 32°C. The cells were then incubated at 39.5°C for 2.5 h, followed by 45 (*A–D*) or 90 min (*E* and *F*) at permissive temperature (32°C). Double-staining experiments were performed to visualize surface VSV-G and intracellular VSV-G in the same cells (*A* and *B*; *C* and *D*; *E* and *F*). In *B*, *D*, and *F*, surface VSV-G was stained after fixation of the cells. In *A*, *C*, and *E*, intracellular VSV-G was stained after permeabilization of the cells. Bar, 10 μm.

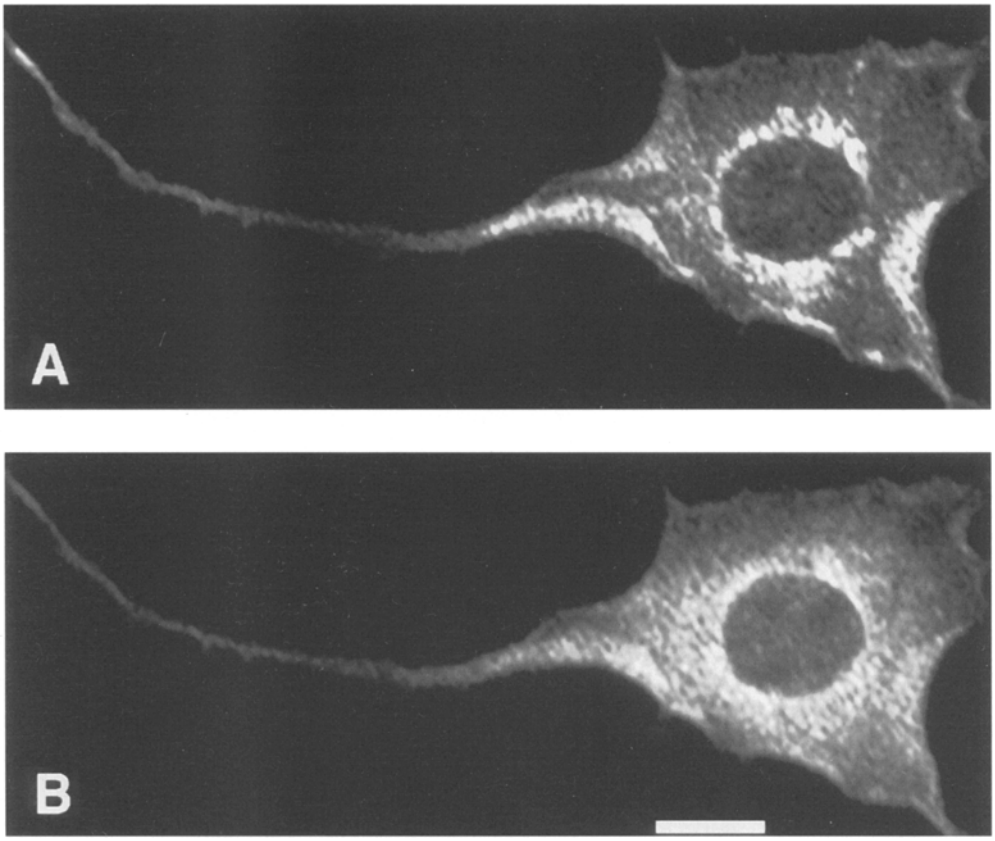

Figure 7. Distribution of HA and VSV-G in BHK clone **a** cells. BHK clone **a** cells were infected with vT7 virus and transfected with VSV-G (*A*) and HA (*B*) plasmids. Cycloheximide was added 3 h after transfection, and after 30 min, the cells were fixed, permeabilized, and doubly stained with anti-HA antibodies and anti-VSV–G antibodies. Bar, 10 μm.

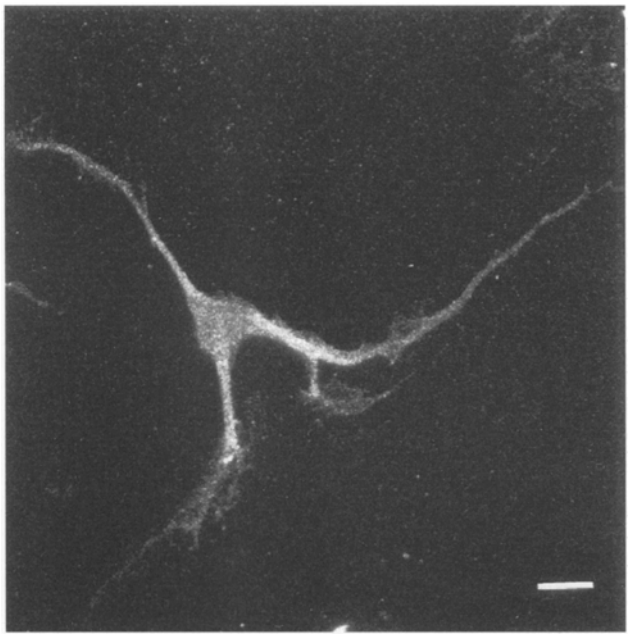

Figure 8. Delivery of newly synthesized influenza ts61 HA to the cell surface in BHK clone **a** cells. BHK clone **a** cells were grown on coverships and infected with influenza ts61 for 1 h at 32°C. The cells were then incubated for 3 h at 40°C, followed by 90 min at 20°C and 20 min at 32°C, the latter two incubations with cycloheximide (20 μg/ml). The cells were fixed, permeabilized, and stained with anti-HA. Bar, 10 μm.

expressing wt-Rab8, although the effects were less pronounced (data not shown). These effects were specific to Rab8 because actin reorganization was not observed when Rab5 was expressed in BHK cells, using the vT7 system (data not shown). This is in accordance with the morphological data that showed that neither Rab5 nor Rab10 induced changes in the cell shape.

Because changes in the actin cytoskeleton are often correlated with microtubule rearrangements, we proceeded to analyze whether any changes in the microtubule networks were induced by Rab8 expression. In control cells, and in cells that expressed the Rab8T22N mutant (Fig. 10 *A*), the microtubules formed asters, radiating out of a centrally located microtubule organizing center (MTOC). However, when cells expressed Rab8Q67L (Fig. 10 *D*), a redistribution of the microtubules occurred. The centrally located MTOC often disappeared, leaving a decreased amount of microtubules in the cell body (Fig. 10, *D* and *E*). Most microtubules were concentrated in the processes where they appeared to be bundled.

To find out whether intact microtubules were required for the Rab8-specific actin reorganization, we transfected cells with the Rab8Q67L gene in the presence of nocodazole. This treatment disrupted the microtubules, leaving only a few remnants in the cell body. These cells showed, however, a clear redistribution of actin very similar to that seen without nocodazole (data not shown). This demonstrates that the Rab8-induced actin reorganization is not dependent on intact microtubules. However, these cells did not develop long processes; instead, they contained numerous short protrusions, suggesting that both actin and

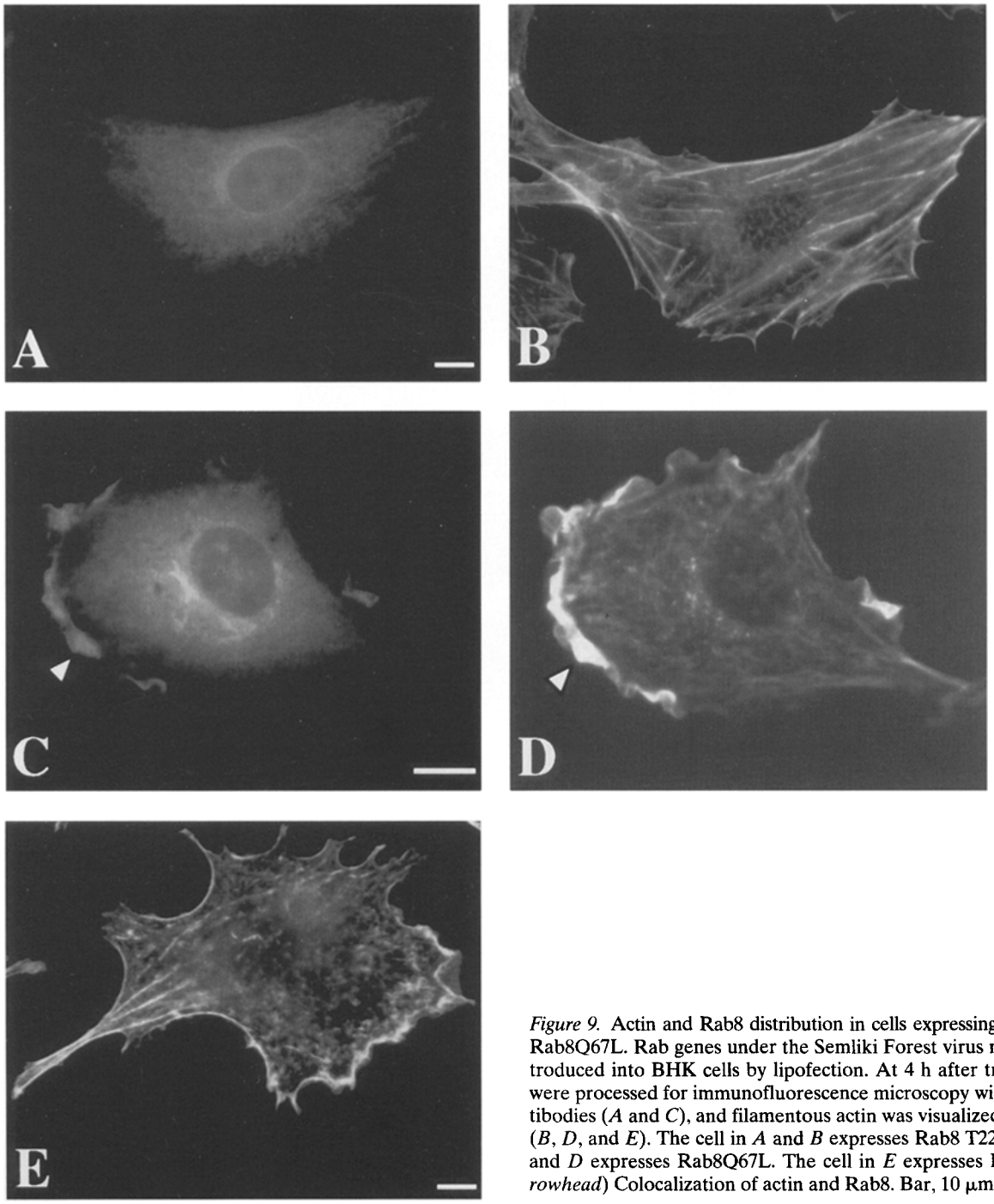

Figure 9. Actin and Rab8 distribution in cells expressing Rab8T22N and Rab8Q67L. Rab genes under the Semliki Forest virus replicon were introduced into BHK cells by lipofection. At 4 h after transfection, cells were processed for immunofluorescence microscopy with anti-Rab8 antibodies (*A* and *C*), and filamentous actin was visualized with phalloidin (*B*, *D*, and *E*). The cell in *A* and *B* expresses Rab8 T22N. The cell in *C* and *D* expresses Rab8Q67L. The cell in *E* expresses Rab8Q67L. (*Arrowhead*) Colocalization of actin and Rab8. Bar, 10 μm.

microtubules are necessary for further elongation of the processes. Cytochalasin D treatment, which inhibits actin polymerization, prevented cell surface outgrowths in Rab8-expressing cells, indicating that actin reorganization is required for the Rab8-induced phenotype (data not shown).

Our previous analysis had demonstrated that the morphological changes induced by Rab8Q67L expression but not by Rab8T22N were also seen in stable cell lines overexpressing the Rab8Q67L protein. We analyzed the F-actin and microtubule distribution in the BHK clone **a** cell line. In contrast with control cells (Fig. 11 *A*) that exhibited actin stress fibers and an MTOC with radiating microtubules (Fig. 11 *B*), Rab8Q67L-expressing cells showed peripheral actin bundles that continued into the processes, whereas stress fibers were almost absent (Fig. 11, *C* and *E*). Cells with ruffles and lamellipodia were also observed. Furthermore, these cells had microtubule bundles in the cell processes, while the MTOC was difficult to distinguish (Fig. 11, *D* and *F*). Taken together, these data demonstrate that activated Rab8 promotes both cytoskeleton reorganization and process outgrowth in fibroblasts not only during transient overexpression but also in stable transfectants.

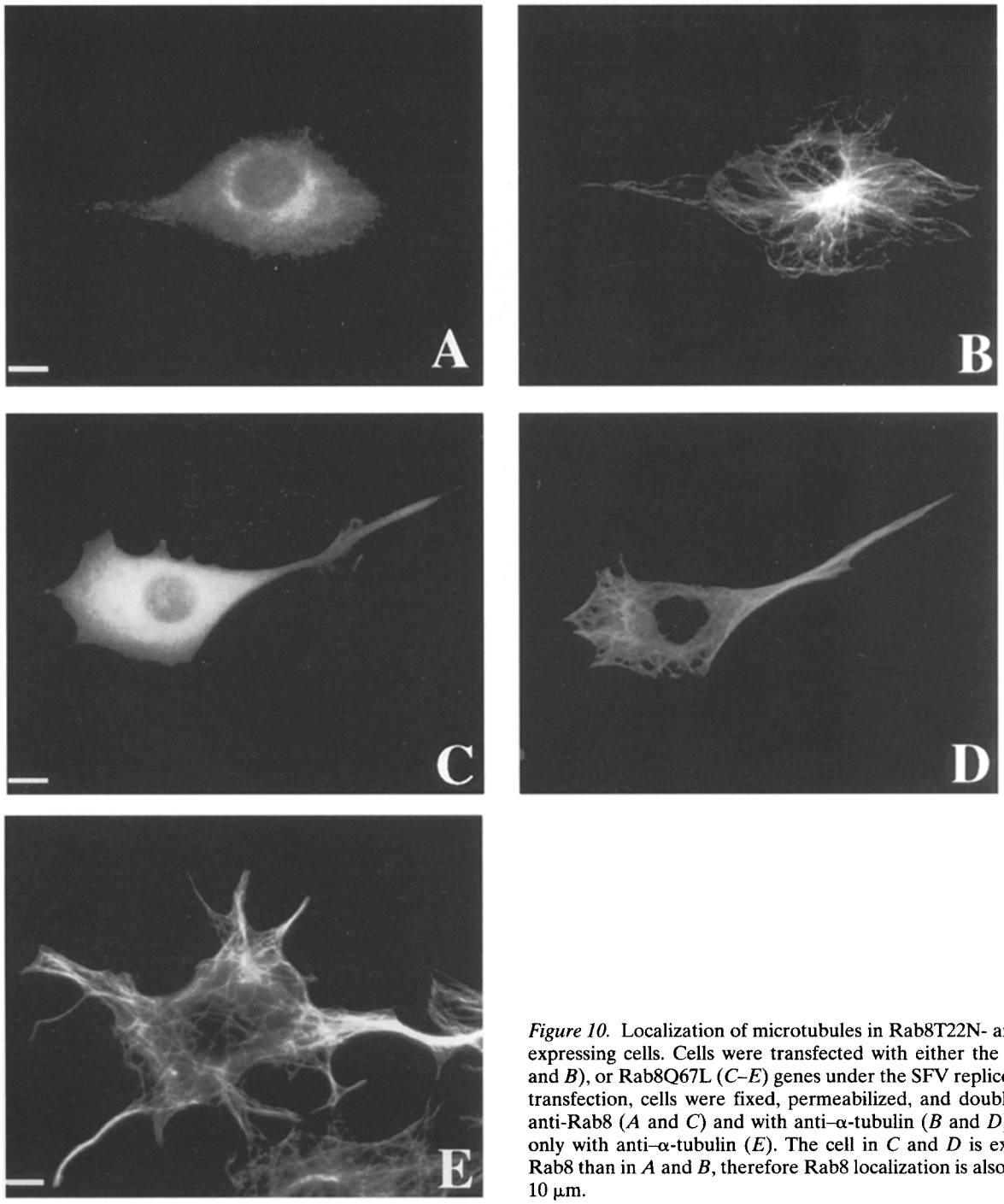

Figure 10. Localization of microtubules in Rab8T22N- and Rab8Q67L-expressing cells. Cells were transfected with either the Rab8T22N (*A* and *B*), or Rab8Q67L (*C–E*) genes under the SFV replicon. At 4 h after transfection, cells were fixed, permeabilized, and doubly stained with anti-Rab8 (*A* and *C*) and with anti–α-tubulin (*B* and *D*), or visualized only with anti–α-tubulin (*E*). The cell in *C* and *D* is expressing more Rab8 than in *A* and *B*, therefore Rab8 localization is also cytosolic. Bar, 10 μm.

Discussion

The surprising finding of this study is that the overexpression of active Rab8 leads to a dramatic change in the morphology of BHK cells. The actin and the microtubule cytoskeletons are reorganized to form cell protrusions into which newly synthesized (basolateral) VSV-G is preferentially delivered. These cell membrane outgrowths are clearly manifestations of Rab8 expression; expression of two other Rab proteins, Rab 5 and 10, did not change cell shape. Our data provide a first molecular link between biosynthetic membrane traffic and process outgrowth. Particularly intriguing is that the two post-Golgi routes present in BHK cells were differentially regulated with respect to delivery into the cell protrusions. In contrast with the basolateral cognate route, the apical cognate route seemed to deliver cargo more randomly over the BHK cell surface.

What could be the mechanism of the Rab8 effect? We have shown previously that basolateral delivery in MDCK cells depends on *N*-ethylmaleimide–sensitive factor, SNAP, and SNARE proteins, while the apical transport route makes use of sphingolipid-cholesterol rafts, VIPs, and annexin 13b (Ikonen et al., 1995; Fiedler et al., 1995). This

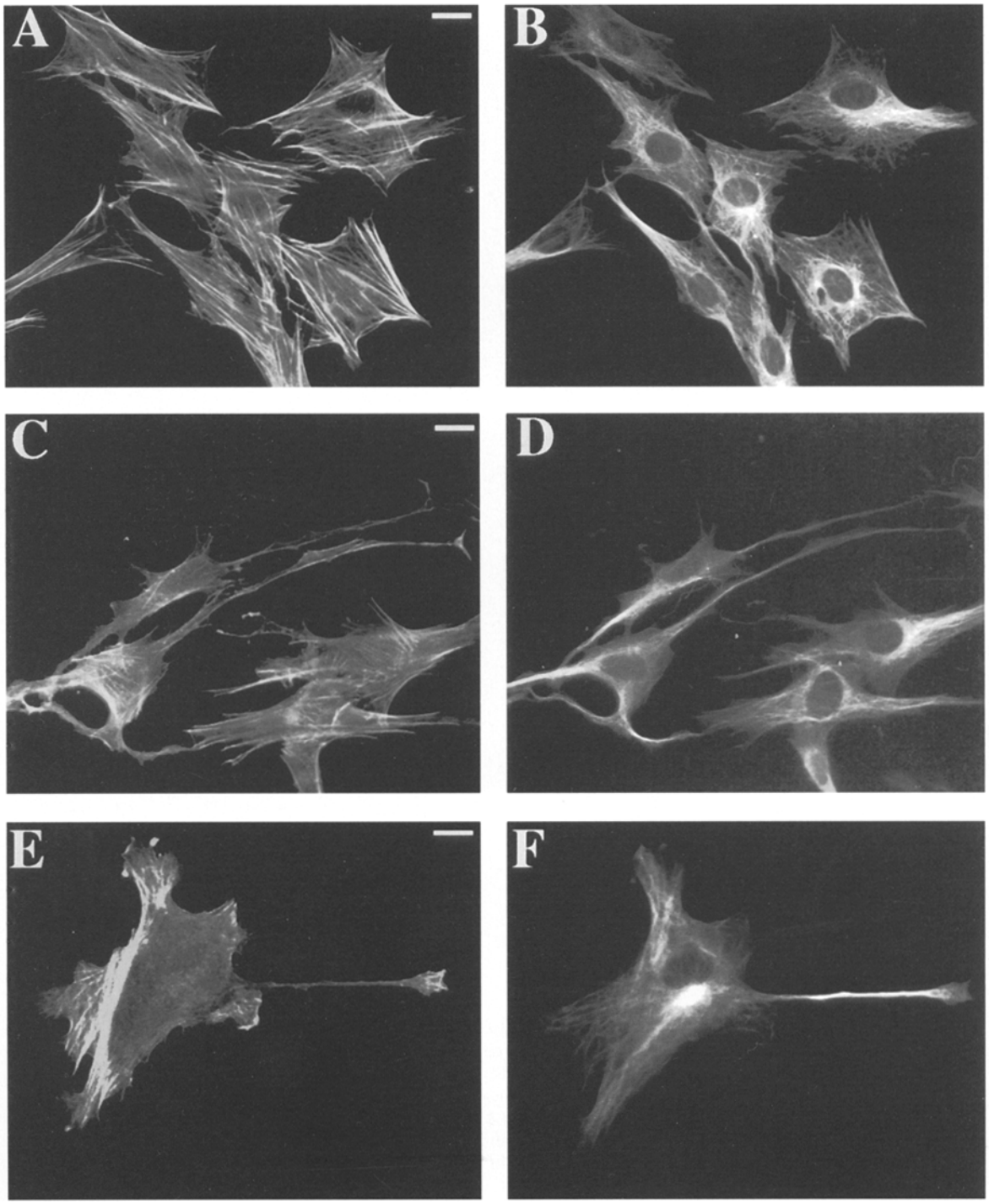

Figure 11. Localization of actin filaments and tubulin in BHK cells and BHK clone **a** cells expressing RabQ67L mutant protein. Cells were grown on coverslips, fixed, and then double staining was performed. Filamentous actin was stained with fluorescent phalloidin (*A*, *C*, and *E*) and tubulin (*B*, *D*, and *F*) by monoclonal anti–α-tubulin antibody. BHK cells (*A* and *B*) were compared with BHK clone **a** cells (*C–F*). Bar, 10 μm.

SNARE machinery is postulated to dock transport vesicles to the target membrane through the interaction of vesicular and target membrane proteins termed v-SNAREs and t-SNAREs (Söllner et al., 1993; Rothman, 1994). Exactly how Rab proteins function in vesicular delivery is not yet clear. They have been proposed to confer specificity to each vesicular trafficking event by regulating SNARE complex assembly (Lian et al., 1994; Søgaard et al., 1994) and/or disassembly after fusion has occurred (Stenmark et al., 1994). However, it is also possible that Rab proteins could be involved in the formation of complexes with other proteins. Such a complex has been found in yeast for Sec4p, the Rab8 homolog, containing Sec6p, Sec8p, and Sec15p in a 19.5 S particle (TerBush and Novick, 1995). A

different complex has been identified for Rab5 in mammalian cells containing rababtin-5 and other uncharacterized proteins (Stenmark et al., 1995). The 19.5 S particle that interacts with Sec4p has been localized to the cytosol and to the tip of the yeast bud where Sec4p-containing vesicles dock and fuse. Interestingly, the Sec4p-containing vesicles require actin filaments for the polarized delivery into the yeast bud (Bretscher et al., 1994). Recently, mammalian homologs, rSec6p and rSec8p, of yeast Sec6p and Sec8p have been characterized (Ting et al., 1995). Immunolocalization of rSec8 in Cos cells showed that the protein was present in plasma membrane ruffles, but the function of these different subunits of the 19.5 S particle is not yet known. However, one of these proteins could be a regulatory actin-binding protein.

Expression of Rab8Q67L induced the formation of polarized surface domains, suggesting that the GTP-bound form of Rab8 is the active species. The appearance of Rab8 in cell processes suggests that translocation of Rab8 to the cell surface is important for the formation of these plasma membrane outgrowths. In agreement with our results, Chen et al. (1993) also observed that Rab8 localizes to ruffles in CHO cells. Thus, it is likely that an accumulation of Rab8 on the plasma membrane is essential for initiating polarized membrane transport. Under nonpolarizing conditions, the Rab8 GTP form would be rapidly hydrolyzed and removed from the target membrane by Rab GDP-dissociation inhibitor and cycled back to initiate a new cycle as suggested in the Sec4p model (Ferro-Novick and Novick, 1993). Reduced GTP hydrolysis could lead to a block in the cycle by leaving Rab8 with its interacting protein complex on the plasma membrane after vesicle fusion. This local accumulation of Rab8 would directly or indirectly promote the formation of actin filaments at this site of the plasma membrane. As a result of the increased polymerization of actin, the cell surface would be pushed out into a cell protrusion. How the basolateral cognate vesicles become routed into these cell surface outgrowths is not clear. Bergman et al. (1983) have previously observed preferential VSV-G delivery into the leading edge of motile fibroblasts. Microtubules directed to the leading edge in fibroblasts are more stabilized than those oriented elsewhere from the MTOC (Gundersen and Bulinski, 1988). The stable microtubules could function as tracks for vesicular delivery. We observed extension of microtubules into the cell processes, and these probably provided the tracks for the increased delivery. This reorganization was so dramatic that it often led to the depletion of microtubules from the cell body. The fact that we saw an accumulation of VSV-G at the end of the processes might be due to a jam of vesicles awaiting a docking opportunity.

How the sequence of events that we have observed after Rab8Q67L expression reflects what takes place during normal fibroblast physiology is not yet known. Our working model would predict that the formation of a normal cell protrusion must be a tightly regulated process that could be initiated by a signal transduction event induced by chemotaxis or substratum interactions that would result in local inactivation of a Rab GAP or activation of a Rab guanine nucleotide exchange factor to produce a local accumulation of Rab8GTP on the cell surface to initiate the formation of surface outgrowth. The preferential delivery of basolateral cognate transport vesicles into the cell protrusions is interesting because this would ensure delivery not only of lipid to the growing membrane process but also of proteins, such as integrins (basolateral in MDCK cells), involved in adhesive events important for regulating cell locomotion (Lauffenberg and Horwitz, 1996; Mitchison and Cramer, 1996). Interesting in this respect is that brefeldin A, which blocks biosynthetic traffic to the cell surface, inhibits directed cell migration (Bershadsky and Futerman, 1994).

The appearance of surface protrusions in Rab8-expressing cells is surprising because these structures have been considered to be induced specifically by different Rho family proteins (Nobes and Hall, 1995). In fibroblasts, Cdc42 stimulates the formation of filopodia, Rac1 promotes the generation of lamellipodia and ruffles, and Rho proteins induce the assembly of focal adhesions and of actin stress fibers. All these morphological changes are associated with a reorganization of the actin cytoskeleton. Moreover, it has been shown that the members of the Rho family can cross talk with each other (Nobes and Hall, 1995). How the Rho family GTPases cross talk with Rab8 is an open question. It is also unclear how the morphology of the plasma membrane outgrowths is determined. Filopodia that are needle-shaped contain a single bundle of unipolar actin filaments, while lamellipodia and cylindrical cell processes contain networks of F-actin. One possibility is that Rab8 functions upstream from the Rho family cascades. If so, it could be equivalent to Rsr-1p (Bud1p), which is a Ras-type GTPase that is required for bud site selection in *S. cerevisiae* but not for bud site assembly that is regulated by Cdc42p (Bender and Pringle, 1989; Johnson and Pringle, 1990; Chant and Herskowitz, 1991). How post-Golgi vesicular traffic is coupled to bud morphogenesis is not yet known. We consider it most likely that the formation of a membrane outgrowth into which VSV-G–containing vesicles preferentially move from the Golgi complex involves a complex cross talk between GTPases of both the Rho family type and Rab8, affecting actin and microtubular organization and dynamics.

In this context, it is very interesting to note that Rac and Cdc42 as well as Rab8 have been shown to regulate neurite outgrowth during neuronal differentiation. Mutants of Drac1 inhibit axon formation in *Drosophila* embryos, while Dcdc42 mutants affect both axon and dendrite outgrowth (Luo et al., 1994). Depletion of Rab8 in rat hippocampal neurons in culture by antisense oligonucleotide treatment results in a decreased number of anterogradely transported vesicles and inhibition of neurite outgrowth (Huber et al., 1995). In dorsal root ganglion cells, the extension of neurites is dependent on continuous anterograde vesicle traffic along microtubules (Martenson et al., 1993). The long processes that sometimes were seen as a result of Rab8Q67L expression in BHK cells (Fig. 7) in fact very much resemble the appearance of an extending neurite, having lengths of >100 μm and a growth cone–like structure at the end of the process.

The presence of Rab8 in most cell types implies a general role for Rab8 in cell morphogenesis. Rab8 is probably not only involved in cell surface polarization in fibroblasts, epithelia, and neurons. In retinal photoreceptors, Rab8 has been suggested to participate in rod outer segment

disk morphogenesis (Deretic et al., 1995). When a helper T cell contacts an antigen-presenting cell, its actin and microtubule cytoskeleton polarizes toward the contact area between the cells under the control of Cdc42 (Stowers et al., 1995). It would be interesting to know whether outgoing biosynthetic traffic also becomes polarized during this process. Our working model for Rab8 involvement in cell surface polarization presents a missing link between the cytoskeletal machinery and the outgoing membrane traffic. The challenge for the future will be to identify how these processes are exactly connected to each other on the molecular level. One important question will be to find out how the delivery through the apical and basolateral cognate routes is spatially regulated.

We thank Frank Bradke for help with the video microscopy, and Suzanne Eaton, Michael Glotzer, Tony Hyman, and Michael Way for valuable comments. We also thank the members of the Simons lab for help and advice.

This work was supported by Deutsche Forschungsgemeinschaft (DFG) (SFB32); J. Peränen and P. Auvinen were supported by the Human Capital and Mobility EC-program. R. Wepf was supported by DFG grant Za 173/2-1.

Received for publication 10 May 1996 and in revised form 8 July 1996.

References

Bender, A., and J.R. Pringle. 1989. Multicopy suppression of the cdc24 budding defect in yeast by CDC42 and three newly identified genes including the ras-related gene RSR1. *Proc. Natl. Acad. Sci. USA.* 86:9976–9980.

Bergman, J.E., A. Kupfer, and S.J. Singer. 1983. Membrane insertion at the leading edge of motile fibroblasts. *Proc. Natl. Acad. Sci. USA.* 83:1367–1371.

Bershadsky, A.D., and A.H. Futerman. 1994. Disruption of the Golgi apparatus by brefeldin A blocks cell polarization and inhibits directed cell migration. *Proc. Natl. Acad. Sci. USA.* 91:5686–5689.

Bordier, C. 1981. Phase separation of integral proteins in Triton X-114 solution. *J. Biol. Chem.* 256:1604–1607.

Brändli, A.W., R.G. Parton, and K. Simons. 1990. Transcytosis in MDCK cells: identification of glycoproteins transported bidirectionally between both plasma membrane domains. *J. Cell Biol.* 111:2909–2921.

Bretscher, A., B. Drees, E. Harsay, D. Schott, and T. Wang .1994. What are the basic functions of microfilaments? Insights from studies in budding yeast. *J. Cell Biol.* 126:821–825.

Bucci, C., R.G. Parton, I.H. Mather, H. Stunnenberg, K. Simons, B. Hoflack, and M. Zerial. 1992. The small GTPase rab5 functions as regulatory factor in the early endocytic pathway. *Cell.* 70:715–728.

Burstein, E.S., W.H. Brondyk, and I.G. Macara. 1992. Amino acid residues in the Ras-like GTPase Rab3A that specify sensitivity to factors that regulate the GTP/GDP cycling of Rab3A. *J. Biol. Chem.* 267:22715–22718.

Chant, J., and I. Herskowitz. 1991. Genetic control of bud site selection in yeast by a set of gene products that constitute a morphogenetic pathway. *Cell.* 65: 1203–1213.

Chavrier, P., M. Vingron, C. Sander, K. Simons, and M. Zerial. 1990. Molecular cloning of Ypt/SEC4-related cDNAs from an epithelial cell line. *Mol. Cell. Biol.* 10:6578–6585.

Chen, Y.-T., C. Holcomb, and H.-P.H. Moore. 1993. Expression and localization of two low molecular weight GTP-binding proteins, Rab8 and Rab10, by epitope tag. *Proc. Natl. Acad. Sci. USA.* 90:6508–6512.

Cid-Arregui, A., R.G. Parton, K. Simons, and C.G. Dotti. 1995. Nocodazole-dependent transport and brefeldin A-sensitive processing and sorting of newly synthesized membrane proteins in cultured neurons. *J. Neurosci.* 15: 4259–4269.

Craighead, M.W., S. Bowden, R. Watson, and J. Armstrong. 1993. Function of the ypt2 gene in the exocytic pathway of *Schizosaccharomyces pombe. Mol. Biol. Cell.* 4:1069–1076.

Der, C.J., T. Finkel, and G.M. Cooper. 1986. Biological and biochemical properties of human ras gene mutated at codon 61. *Cell.* 44:167–176.

Deretic, D., L.A. Huber, N. Ransom, M. Mancini, K. Simons, and D.S. Papermaster. 1995. rab8 in retinal photoreceptors may participate in rhodopsin transport and in outer segment disk morphogenesis. *J. Cell Sci.* 108:215–224.

Dotti, C.G., and K. Simons. 1990. Polarized sorting of viral glycoproteins to the axon and dendrites of hippocampal neurons in culture. *Cell.* 62:63–72.

Feig, L.A., and G.M. Cooper. 1988. Inhibition of NIH 3T3 cell proliferation by mutated Ras proteins with preferential affinity for GDP. *Mol. Cell. Biol.* 8: 3235–3243.

Ferro-Novick, S., and P. Novick. 1993. The role of GTP-binding proteins in transport along the exocytic pathway. *Annu. Rev. Cell Biol.* 9:575–599.

Fiedler, K., F. Lafont, R.G. Parton, and K. Simons. 1995. Annexin XIIIb: a novel epithelial specific annexin is implicated in vesicular traffic to the apical plasma membrane. *J. Cell Biol.* 128:1043–1053.

Fuerst, T.R., E.G Niles, F.W. Studier, and B. Moss. 1986. Eukaryotic transient-expression system based on recombinant vaccinia virus that synthesizes bacteriophage T7 RNA polymerase. *Proc. Natl. Acad. Sci. USA.* 83:8122–8126.

Glotzer, M., and A.A. Hyman. 1995. The importance of being polar. *Curr. Biol.* 5:1102–1105.

Gottlieb, T.A., I.E. Ivanov, M. Adesnik, and D.D. Sabatini. 1993. Actin microfilaments play a critical role in endocytosis at the apical but not the basolateral surface of polarized epithelial cells. *J. Cell Biol.* 120:695–710.

Govindan, B., R. Bower, and P. Novick. 1995. The role of MYO2, a yeast class V myosin, in vesicular transport. *J. Cell Biol.* 128:1055–1068.

Gundersen, G.G., and J.C. Bulinski. 1988. Selective stabilization of microtubules oriented toward the direction of cell migration. *Proc. Natl. Acad. Sci. USA.* 85:5946–5950.

Hasson, T., and M.S. Mooseker. 1995. Molecular motors, membrane movements and physiology: emerging roles for myosins. *Curr. Opin. Cell Biol.* 7: 587–594.

Haubruck, H., U. Engelke, P. Mertins, and D. Gallwitz. 1990. Structural and functional analysis of ypt2, an essential ras-related gene in the fission yeast *Schizzosaccharomyces pombe* encoding a Sec4 protein homologue. *EMBO (Eur. Mol. Biol. Organ.) J.* 9:1957–1962.

Hiti, A.L., A.R. Davis, and D.P. Nayak. 1981. Complete sequence analysis shows that the hemagglutinins of the H0 and H2 subtypes of human influenza virus are closely related. *Virology.* 111:113–124.

Ho, S.N., H.D. Hunt, R.M. Horton, J.K. Pullen, and L.R. Pease. 1989. Site-directed mutagenesis by overlap extension using the polymerase chain reaction. *Gene (Amst.).* 77:51–59.

Huber, L.A., M.J. De Hoop, P. Dupree, M. Zerial, K. Simons, and C.G. Dotti. 1993*a*. Protein transport to the dendritic plasma membrane of cultured neurons is regulated by rab8p. *J. Cell Biol.* 123:47–55.

Huber, L.A., S. Pimplikar, R.G. Parton, H. Virta, M. Zerial, and K. Simons. 1993*b*. rab8, a small GTPase involved in vesicular traffic between TGN and the basolateral plasma membrane. *J. Cell Biol.* 123:35–45.

Huber, L.A., P. Dupree, and C.G. Dotti. 1995. A deficiency of small GTPase rab8 inhibits membrane traffic in developing neurons. *Mol. Cell. Biol.* 15: 918–924.

Ikonen, E., M. Tagaya, O. Ullrich, C. Montecucco, and K. Simons. 1995. Different requirements for NSF, SNAP, and Rab proteins in apical and basolateral transport in MDCK cells. *Cell.* 81:571–580.

Johnson, D. I., and J. R. Pringle. 1990. Molecular characterization of CDC42, a *Saccharomyces cerevisiae* gene involved in the development of cell polarity. *J. Cell Biol.* 111:143–152.

Kelly, R.B. 1990. Microtubules, membrane traffic and cell organization. *Cell.* 61:5–7.

Kreis, T.E. 1986. Microinjected antibodies against the cytoplasmic domain of vesicular stomatitis virus glycoprotein block its transport to the cell surface. *EMBO (Eur. Mol. Biol. Organ.) J.* 5:931–941.

Lafont, F., J.K. Burkhardt, and K. Simons. 1994. Involvement of microtubule motors in basolateral and apical transport in kidney cells. *Nature (Lond.).* 372:801–803.

Langford, G.M. 1995. Actin- and microtubule-dependent organelle motors: interrelationships between the two motility systems. *Curr. Opin. Cell Biol.* 7: 82–88.

Lauffenberg, D.A., and A.F. Horwitz. 1996. Cell migration: a physical integrated molecular process. *Cell.* 84:359–369.

Lian, J.P., S. Stone, Y. Jiang, P. Lyons, and S. Ferro-Novick. 1994. Ypt1p implicated in v-SNARE activation. *Nature (Lond.).* 372:698–701.

Liljeström, P., and H. Garoff. 1991. A new generation of animal cell expression vectors based on the Semliki Forest virus replicon. *BioTechnology.* 9:1356–1361.

Luo, L., Y.J. Liao, L.Y. Jan, and Y.N. Jan. 1994. Distinct morphogenetic functions of similar small GTPases: *Drosophila* Drac1 is involved in axonal outgrowth and myoblast fusion. *Genes & Dev.* 8:1787–1802.

Martenson, C., K. Stone, M. Reedy, and M. Sheetz. 1993. Fast axonal transport is required for growth cone advance. *Nature (Lond.).* 366:66–69.

Mitchison, T.J., and L.P. Cramer. 1996. Actin-based cell motility and cell locomotion. *Cell.* 84:371–379.

Muallem, S., K. Kwiatkowska, X. Xu, and H.L. Yin. 1995. Actin filament disassembly is a sufficient final trigger for exocytosis in nonexcitable cells. *J. Cell Biol.* 128:589–598.

Nelson, W.J. 1992. Regulation of cell surface polarity from bacteria to mammals. *Science (Wash. DC).* 258:948–955.

Nobes, C.D., and A. Hall. 1995. Rho, Rac, and Cdc42 GTPases regulate the assembly of multimolecular focal complexes associated with actin stress fibers, lamellipodia, and filopodia. *Cell.* 81:53–62.

Novick, P., and P. Brennwald. 1993. Friends and family: the role of the Rab GTPases in vesicular transport. *Cell.* 75:597–601.

Peränen, J. 1992. Rapid biotinylation and affinity purification of antibodies. *Biotechniques.* 13:545–547.

Rindler, M.J., I.E. Ivanov, and D.D. Sabatini. 1987. Microtubule-acting drugs lead to the nonpolarized delivery of the influenza hemagglutinin to the cell surface of polarized Madin-Darby canine kidney cells. *J. Cell Biol.* 104:231–241.

Rodriguez-Boulan, E., and S.K. Powell. 1992. Polarity of epithelial and neuronal cells. *Annu. Rev. Cell Biol.* 8:395–427.

Rogalski, A.A., J.E. Bergman, and S.J. Singer. 1984. Effect of microtubule assembly status on the intracellular processing and surface expression of an integral protein of the plasma membrane. *J. Cell Biol.* 99:1101–1109.

Rose, J.K., and J.E. Bergman. 1983. Altered cytoplasmic domains affect intracellular transport of vesicular stomatitis virus glycoprotein. *Cell.* 34:513–524.

Rothman, J.E. 1994. Mechanisms of intracellular protein transport. *Nature (Lond.).* 372:55–63.

Sauve, D.M., D.T. Ho, and M. Roberge. 1995. Concentration of dilute protein for gel electrophoresis. *Anal. Biochem.* 226:382–383.

Simons, K., and A. Wandinger-Ness. 1990. Polarized sorting in epithelia. *Cell.* 62:207–210.

Simons, K., P. Dupree, K. Fiedler, L.A. Huber, T. Kobayashi, T. Kurzchalia, V. Olkkonen, S. Pimplikar, R.G. Parton, and C.G. Dotti. 1992. Biogenesis of cell-surface polarity in epithelial cells and neurons. *Cold Spring Harbor Symp. Quant. Biol.* 57:611–619.

Singer, S.J., and A. Kupfer. 1986. The directed migration of eukaryotic cells. *Annu. Rev. Cell Biol.* 2:337–365.

Søgard, M., K. Tani, R. Ruby Ye, S. Geromanos, P. Tempst, T. Kirchausen, J.E. Rothman, and T. Söllner. 1994. A Rab protein is required for the assembly of SNARE complexes in the docking of transport vesicles. *Cell.* 78:937–948.

Söllner, T., S.W. Whiteheart, M. Brunner, H. Erdjument-Bromange, S. Geromanos, P. Tempst, and J.E. Rothman. 1993. SNAP receptors implicated in vesicle targeting and fusion. *Nature (Lond.).* 362:318–324.

Stenmark, H., R.G. Parton, O. Steele-Mortimer, A. Lutcke, J. Gruenberg, and M. Zerial. 1994. Inhibition of rab5 GTPase activity stimulates membrane fusion and endocytosis. *EMBO (Eur. Mol. Biol. Organ.) J.* 13:1287–1296.

Stenmark, H., G. Vitale, O. Ullrich, and M. Zerial. 1995. Rabaptin-5 is a direct effector of the small GTPase Rab5 in the endocytic membrane fusion. *Cell.* 83:423–432.

Stowers, L., D. Yelon, L.J. Berg, and J. Chant. 1995. Regulation of the polarization of T cells toward antigen-presenting cells by Ras-related GTPase CDC42. *Proc. Natl. Acad. Sci. USA.* 92:5027–5031.

TerBush, D.R., and P. Novick. 1995. Sec6, Sec8, and Sec15 are components of a multisubunit complex which localizes to small bud tips in *Saccharomyces cerevisiae. J. Cell Biol.* 130:299–312.

Ting, A.E., C.D. Hazuka, S.-C. Hsu, M.D. Kirk, A.J. Bean, and R. Scheller. 1995. rSec6 and rSec8, mammalian homologs of yeast proteins essential for secretion. *Proc. Natl. Acad. Sci. USA.* 92:9613–9617.

Vitale, M.L., E.P. Seaward, and J.-M. Trifaro. 1995. Chromaffin cell cortical actin network dynamics control the size of release-ready vesicle pool and the initial rate of exocytosis. *Neuron.* 14:353–363.

Wandinger-Ness, A., M.K. Bennett, C. Antony, and K. Simons. 1990. Distinct transport vesicles mediate the delivery of plasma membrane proteins to the apical and basolateral domains of MDCK cells. *J. Cell Biol.* 111:987–1000.

Yoshimori, T., P. Keller, M.G. Roth, and K. Simons. 1996. Different biosynthetic transport routes to the plasma membrane in BHK and CHO cells. *J. Cell Biol.* 133:247–256.

Zerial, M., and H. Stenmark. 1993. Rab GTPases in vesicular transport. *Curr. Opin. Cell Biol.* 5:613–620.